Research Article

Exosomes derived from bone marrow mesenchymal stem cells protect the injured spinal cord by inhibiting pericyte pyroptosis

https://doi.org/10.4103/1673-5374.314323

Date of submission: July 31, 2020

Date of decision: November 3, 2020

Date of acceptance: April 6, 2021

Date of web publication: June 7, 2021

Yan Zhou[1, #], Lu-Lu Wen[2, #], Yan-Fei Li[2], Kai-Min Wu[2], Ran-Ran Duan[2], Yao-Bing Yao[2], Li-Jun Jing[2], Zhe Gong[2], Jun-Fang Teng[2], Yan-Jie Jia[2, *]

Graphical Abstract *Bone marrow mesenchymal stem cells-derived exosomes (BMSC-EXOs) may play a crucial role in protecting the spinal cord through inhibition of pericyte pyroptosis in vivo and in vitro*

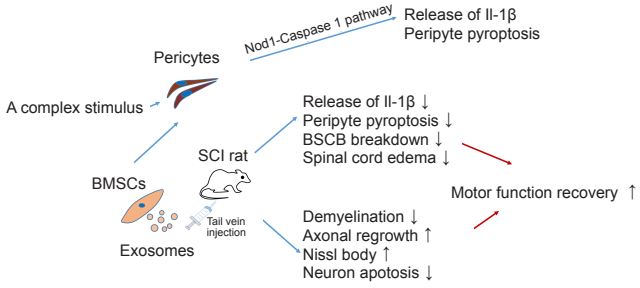

Abstract

Mesenchymal stem cell (MSC) transplantation is a promising treatment strategy for spinal cord injury, but immunological rejection and possible tumor formation limit its application. The therapeutic effects of MSCs mainly depend on their release of soluble paracrine factors. Exosomes are essential for the secretion of these paracrine effectors. Bone marrow mesenchymal stem cell-derived exosomes (BMSC-EXOs) can be substituted for BMSCs in cell transplantation. However, the underlying mechanisms remain unclear. In this study, a rat model of T10 spinal cord injury was established using the impact method. Then, 30 minutes and 1 day after spinal cord injury, the rats were administered 200 μL exosomes via the tail vein (200 μg/mL; approximately 1×10^6 BMSCs). Treatment with BMSC-EXOs greatly reduced neuronal cell death, improved myelin arrangement and reduced myelin loss, increased pericyte/endothelial cell coverage on the vascular wall, decreased blood-spinal cord barrier leakage, reduced caspase 1 expression, inhibited interleukin-1β release, and accelerated locomotor functional recovery in rats with spinal cord injury. In the cell culture experiment, pericytes were treated with interferon-γ and tumor necrosis factor-α. Then, Lipofectamine 3000 was used to deliver lipopolysaccharide into the cells, and the cells were co-incubated with adenosine triphosphate to simulate injury *in vitro*. Pre-treatment with BMSC-EXOs for 8 hours greatly reduced pericyte pyroptosis and increased pericyte survival rate. These findings suggest that BMSC-EXOs may protect pericytes by inhibiting pyroptosis and by improving blood-spinal cord barrier integrity, thereby promoting the survival of neurons and the extension of nerve fibers, and ultimately improving motor function in rats with spinal cord injury. All protocols were conducted with the approval of the Animal Ethics Committee of Zhengzhou University on March 16, 2019.

Key Words: blood-spinal cord barrier; edema; exosome; pericyte; NOD1; pro-caspase 1; pyroptosis; spinal cord injury

Chinese Library Classification No. R456; R745.4; R363

Introduction

Spinal cord injury (SCI) is a life-threatening traumatic injury often accompanied by paraplegia, neurological complications, and reduced life expectancy (Rahimi-Movaghar et al., 2013). After the primary traumatic event, a cascade of secondary injury events start, which includes, but is not limited to, ischemia, hemorrhage, breakdown of the blood-spinal cord barrier (BSCB), edema, neuroinflammation and oxidative stress. These processes ultimately accelerate neuronal loss and axonal degeneration (Aslan et al., 2009; Haque et al., 2017). Among these, breakdown of the BSCB and neuroinflammation are key events in the pathogenesis of SCI, and make recovery of normal functioning of the spinal cord more difficult (Pan et al., 2019).

Pericytes are mural cells inserted in the basement membrane of microvessels throughout the body, including the spinal cord. Numerous preclinical studies have demonstrated that pericytes, a central component of the neurovascular unit, have critical functions, including the regulation of BSCB/blood-brain barrier permeability and capillary blood flow,

[1]Department of Radiology, The First Affiliated Hospital of Zhengzhou University, Zhengzhou, Henan Province, China; [2]Department of Neurology, The First Affiliated Hospital of Zhengzhou University, Zhengzhou, Henan Province, China

*Correspondence to: Yan-Jie Jia, PhD, jiayanjie1971@edu.zzu.cn.

https://orcid.org/0000-0002-2220-9257 (Yan-Jie Jia); https://orcid.org/0000-0001-9571-6295 (Yan Zhou); https://orcid.org/0000-0002-9225-5443 (Lu-Lu Wen)

#Both authors contributed equally to this work.

Funding: *This work was supported by the National Natural Science Foundation of China, No. U1604170 (to YJJ).*

How to cite this article: *Zhou Y, Wen LL, Li YF, Wu KM, Duan RR, Yao YB, Jing LJ, Gong Z, Teng JF, Jia YJ (2022) Exosomes derived from bone marrow mesenchymal stem cells protect the injured spinal cord by inhibiting pericyte pyroptosis. Neural Regen Res 17(1):194-202.*

the development and maintenance of the vascular system, clearance of toxic molecules, and the regulation of the entry of immune cells into the central nervous system (Berthiaume et al., 2018; Hashitani et al., 2018; Hashitani and Mitsui, 2019). A reduction in pericytes contributes to increased BSCB permeability, microcirculatory disruption, and the leakage of harmful blood components into the central nervous system, thereby aggravating neurological dysfunction (Wu et al., 2014).

Previous studies have suggested that acute inflammatory responses after SCI cause severe tissue damage when cellular debris and released intracellular proteins stimulate inflammatory cells, including resident microglia and astrocytes, as well as blood neutrophils, macrophages, B lymphocytes and T lymphocytes recruited from the circulatory system (David and Kroner, 2011; Orr and Gensel, 2018; Ungerer et al., 2020). Some cell types such as pericytes and neurons can also secrete pro-inflammatory cytokines.

Pyroptosis is a recently identified form of programmed cell death that is dependent on the activation of caspases 1, 4, 5 and 11, and induces the release of pro-inflammatory cytokines (Bergsbaken et al., 2009; Tan et al., 2021). Recently, Li et al. (2018) found that pericyte loss caused by pyroptosis, rather than apoptosis, leads to vascular leakage and mortality in an animal model of sepsis induced by cecal ligation and puncture. Previous studies indicate that inhibition of pyroptosis promotes motor functional recovery after SCI (Dai et al., 2019; Zheng et al., 2019). Thus, pyroptosis may also result in pericyte loss and BSCB permeability changes in SCI models. Further study is needed to clarify the role of pericytes in inflammation.

Mesenchymal stem cells (MSCs) derived from various sources have been reported to be a promising treatment strategy in preclinical and clinical studies of cell-based therapies (Huang et al., 2018; Mahmoudi et al., 2019; Yi et al., 2019; Wei et al., 2021). However, the therapeutic benefits of MSCs are limited by shortcomings, including poor survival rates, possible tumor formation, immunological rejection, and genetic variation (Hoogduijn et al., 2011; Moya et al., 2018). Previous studies have shown that the therapeutic effects of MSCs mainly depend on their release of paracrine soluble factors rather than their direct differentiation into injured cell types (Zhang et al., 2018; Yaghoubi et al., 2019). Exosomes (40–120 nm in diameter) are essential for the release of MSC-derived paracrine factors. Exosomes contain numerous key signaling molecules that are protected from degradation by the lipid bilayer packaging (Phinney et al., 2015). Emerging reports suggest that exosomes from MSCs promote recovery from traumatic brain injury, neuropathic pain and SCI (Kalani and Tyagi, 2015; Xiong et al., 2017; Gao et al., 2018). A novel study recently showed that embryonic stem cell derived-exosomes reduce inflammation-induced pyroptosis in doxorubicin-induced cardiomyopathy (Tavakoli Dargani and Singla, 2019). However, the effects of bone MSC-derived exosomes (BMSC-EXOs) on pyroptosis in spinal cord injury remain unknown. Therefore, in the present study, we test the hypothesis that BMSC-EXOs play a critical role in protecting the spinal cord through the inhibition of pericyte pyroptosis *in vivo* and *in vitro*.

Materials and Methods

BMSC-EXO isolation

According to a previously published protocol (Li et al., 2019), male Sprague-Dawley rats (2 months old, specific-pathogen-free grade, purchased from Huaxing Company, Zhengzhou, China, license No. SCXK(Yu)2019-0002) were anesthetized by 4% isoflurane (RWD, Shenzhen, China) inhalation and sacrificed by decapitation (**Table 1**). The tibias were stripped to collect bone marrow cells. Then, the cell suspension was centrifugated at 1000 × *g* for 5 minutes, and cell pellets were collected and resuspended in complete medium, consisting of Dulbecco's modified Eagle medium (DMEM; Thermo Fisher Scientific, Waltham, MA, USA) containing 10% fetal bovine serum (Thermo Fisher Scientific) and penicillin/streptomycin (Leagene Biotechnology, Beijing, China). After changing the complete medium 2 days later, the cells adhering to the culture dish were considered P0 BMSCs. At 80–90% confluence, the cells were digested with ethylenediaminetetraacetic acid-containing trypsin at 37°C for 1 minute. The digestion was terminated with complete medium, and the cell suspension was re-seeded into a dish.

Table 1 | **The sex, age and number of each part of the rat**

	Number	Sex	Age
Bone marrow mesenchymal stem cells-derived exosomes isolation	No record	Male	2 mon
Pericyte isolation	No record	Male	3–5 wk
Basso, Beattie and Bresnahan scores	10/group	Male	3 mon
Immunohistochemical analysis of neurofilament 200; Nissl staining; Fluoro-Jade B; Luxol Fast Blue; hematoxylin and eosin staining; immunofluorescence analysis	6/group	Male	3 mon
Evans blue assessment; *In Vivo* Imaging System	6/group	Male	3 mon
Spinal cord water content measurement; interleukin-1β	6/group	Male	3 mon
Western blot	6/group	Male	3 mon

The same rats in each group were used for immunohistochemical analysis of neurofilament 200, Nissl staining, Fluoro-Jade B, Luxol Fast Blue, hematoxylin and eosin staining, immunofluorescence analysis, vans blue assessment, *In Vivo* Imaging System, spinal cord water content measurement, interleukin-1β, and western blot.

BMSCs at passages 3 to 6 were used to isolate exosomes. BMSCs at 80–90% confluence were cultured in exosome-free complete medium for 2 days, and the conditioned supernatant was collected into an ultracentrifuge tube and centrifuged (successively) at 300 × *g* for 10 minutes, 2000 × *g* for 10 minutes, and 10,000 × *g* for 30 minutes to eliminate cells and debris. Thereafter, filtration through a 0.22-μm filter (Millipore, Burlington, MA, USA) was performed to further reduce dead cells and particles in the supernatant. Exosomes were then separated by ultracentrifugation at 110,000 × *g* for 70 minutes. After discarding the supernatant, the pellet was resuspended in phosphate-buffered saline (PBS), and ultracentrifuged again at 110,000 × *g* for another 70 minutes. Finally, the supernatant was discarded, and the pellet was stored at –80°C until use in experiments. All of these procedures were conducted at 4°C. Nanosight technology (Particle Metrix, Meerbusch, Germany) was used to analyze the size distribution of exosomes.

Transmission electron microscopy examination

Exosomes from BMSCs were resuspended and observed by transmission electron microscopy (Tecnai 12, Philips, Amsterdam, Netherlands) (Wei et al., 2019). Specimens on copper grids were made using two methods: dripping and floating. In the dripping method, the exosome suspension was placed onto the copper mesh for a few seconds. In the floating method, the exosome suspension was placed onto parafilm, and the copper meshes were floated onto the droplet for 3 minutes. Subsequently, the excess liquid was absorbed by filter paper in both methods. All samples were floated in a 1% aqueous solution of phosphotungstic acid for 30 seconds, and air-dried before examination by transmission electron microscopy.

Nanoparticle tracking analysis

The size and concentration of exosomes were evaluated using Nanosight Zeta View PMX 110 (Particle Metrix). A size

distribution plot with particle diameter (nm) on the x-axis and concentration (particles/mL) on the y-axis was made.

BMSC-EXO labeling

According to the manufacturer's instructions, PKH26 dye (Sigma-Aldrich, St. Louis, MO, USA) was used to label exosomes. Briefly, the exosome suspension was incubated with 2 μL PKH26 for 20 minutes at room temperature. Then, the staining reaction was stopped by isovolumetric PBS containing 5% bovine serum albumin (Solarbio, Beijing, China). Labeled exosomes were isolated by ultracentrifugation, as described above.

SCI model and treatment

All experiments complied with the recommendations in the Guide for the Care and Use of Laboratory Animals of the National Institutes of Health. All protocols were conducted with the approval of the Animal Ethics Committee of Zhengzhou University on March 16, 2019. A total of 160 adult male Sprague-Dawley rats (weighing 200–250 g, 3 months old, specific-pathogen-free grade, purchased from HuaXing Company, Zhengzhou, China, license No. SCXK (Yu) 2019-0002) were divided into the following four groups at random: Sham, EXO (Sham + EXO), SCI, and SCI + EXOs (n = 40/group). According to established protocol (Wang et al., 2018), rats were fixed on a fixing plate after anesthesia was induced by inhalation of 4% isoflurane. When the animals lost consciousness, the vertebral column was exposed by separation of the skin, muscle and ligament overlying the appropriate spinal cord region. A T10 laminectomy was conducted, and the exposed spinal cord was subjected to a contusive wound by applying an impact of 2 N (equal to 200 kilodyne) with a spinal cord impactor (IH Impactor; Precision Systems and Instrumentation, Lexington, KY, USA). The sham rats underwent laminectomy without a contusive wound. After surgery, all rats were treated with penicillin for 3 days, and the bladders were manually voided three times a day. In the SCI + EXO group, rats received 200 μL exosomes (200 μg/mL, derived from ~1×10^6 BMSCs) via the tail vein at 30 minutes and 1 day after SCI. Using the same administration route and at the same time points, rats in the EXO group received 200 μL exosomes (200 μg/mL), and rats in the SCI group received 200 μL PBS (**Table 1**).

Histological analysis

At 3 days post injury (dpi), rats were anesthetized by inhalation of 4% isoflurane (RWD Life Science) and perfused with physiological saline. The T10 spinal cords were embedded in paraffin and serially cut into 5-μm-thick coronal sections. Slides were then mounted and stored at 4°C for staining. For Nissl staining, the dewaxed tissue slides were dyed with 1% toluidine blue for 40 minutes at 60°C, dehydrated, and sealed with neutral gum. For Fluoro-Jade B (FJB) staining, slides were incubated with a 0.0004% solution of FJB (Millipore) for 20 min and washed with distilled water three times. FJB-stained cells were then captured on a fluorescence microscope (Olympus, Tokyo, Japan) at 200× magnification, and quantitatively analyzed using ImageJ software (National Institutes of Health, Bethesda, MD, USA). For Luxol Fast Blue staining (Amtul et al., 2021), slides were incubated in 0.1% Luxol Fast Blue stain overnight at 60°C. Thereafter, slides were washed with double-distilled water, and then incubated in 0.05% lithium carbonate for an additional 10 seconds. For hematoxylin and eosin staining, slides were successively stained with hematoxylin and eosin to observe the structural damage according to an established protocol (Xie et al., 2021).

Immunohistochemical analysis

For immunohistochemistry, paraffin sections of T10 spinal cord tissue at 3 dpi were incubated with anti-neurofilament 200 (NF-200) antibody (1:200; mouse, Cat# GB13141; Servicebio, Wuhan, China) overnight at 4°C. Then, the slides were washed with PBS, and goat anti-mouse IgG (1:200; Cat# G1214-100UL; Servicebio) was applied and incubated 1 hour at room temperature. The NF-200 signals were observed with a light microscope (Olympus).

Immunofluorescence analysis

For immunofluorescence of the spinal cord tissues at 3 dpi, tissue slides and round coverslips were blocked with 5% bovine serum albumin for 1 hour, and then incubated with primary antibody overnight at 4°C. The primary antibodies included mouse anti-platelet-derived growth factor receptor (Pdgfr; 1:250; Cat# ab69506; Abcam), mouse anti-caspase 1 (1:250, Cat# sc-398715, Santa Cruz Biotechnology, Santa Cruz, CA, USA), rabbit anti-Nod1 (1:200; Cat# PA5-79747; Invitrogen, Carlsbad, CA, USA), and rabbit anti-CD31 (1:200; Cat# ab24590; Abcam). After washing with PBS three times, the tissues were incubated with the corresponding secondary antibody (IFKine™ Green donkey anti-mouse IgG, 1:300, Cat# A24211, Abbkine, Wuhan, China; Dylight 594, rabbit anti-goat IgG, 1:300, Cat# A23430, Abbkine) for 1 hour at room temperature in the dark. Subsequently, the tissues were stained with 4′,6-diamidino-2-phenylindole (DAPI) for 15 minutes, and images were acquired using fluorescence microscopy (Olympus).

Evans blue assessment

To assess the integrity of the BSCB at 3 dpi, the Evans blue (EB) extravasation assay was conducted as previously described (Xu et al., 2019). About 2% EB (10 mg/mL; Sigma-Aldrich) dissolved in PBS was injected into rats through the tail vein. Then, 2 hours later, the rats were anesthetized with 4% isoflurane and perfused with saline to clear the circulation of EB dye. The spinal cord was dissected, and the dye distribution was imaged using a digital camera. Then, the spinal cord was cut into two parts (T9–10 and T10–11 segments). The T9–10 segments were weighed and soaked in methanamide (Sigma-Aldrich) for 24 hours (80°C). After centrifugation at 20,000 × g for 20 minutes, the supernatant was collected. A spectrophotometer (Nanodrop One, Thermo Fisher Scientific) was used with excitation and emission wavelengths of 620 nm and 680 nm, respectively, to measure the absorbance of the supernatant. The EB dye content was analyzed using an EB standard curve. The T10–11 segments were frozen in optimal cutting temperature compound (Sakura Finetek, Tokyo, Japan), sectioned (20 μm), and stored in a dark container at –20°C before measurement of EB with fluorescence imaging (Olympus).

***In Vivo* Imaging System**

The spinal cords, 3 days after SCI, were processed with 2% EB as mentioned above. Subsequently, the region of interest was manually defined, and images were captured using the *In Vivo* Imaging System (IVIS) Lumina XR optical imager (Perkin Elmer, Waltham, MA, USA) with 620 nm excitation and 680 nm emission filters, auto exposure time, and a binning factor of 2. Fluorescence was expressed as the total or average radiant efficiency of selected regions of interest.

Spinal cord water content measurement

Rats were anesthetized by inhalation of 4% isoflurane, and then perfused with physiological saline. Water content was measured at 3 dpi as previously described (Li et al., 2014; Luo et al., 2015). A 1-cm section of spinal cord along the injury epicenter was obtained and weighed before and after drying for 48 hours at 80°C until a constant weight (dry weight) was achieved. The water content of the spinal cord (%) was calculated as: (wet weight – dry weight)/wet weight × 100.

Basso, Beattie and Bresnahan scores

To assess neurological function, the Basso, Beattie and Bresnahan (BBB) score (Basso et al., 1995) was calculated 1, 3, 7, 14, 21 and 28 days after SCI in the open field. The BBB score

ranges from 0 to 21, which mainly evaluates the joint function hind limb coordination and weight bearing ability; the higher score indicates better motor function.

Enzyme-linked immunosorbent assay

Following the manufacturer's instructions, interleukin-1β (IL-1β) was quantified at 3 dpi with enzyme-linked immunosorbent assay kits. Spinal cord tissues were isolated, homogenized in PBS, and frozen at –20°C overnight. Then, the suspensions were centrifuged at 12,000 × *g* for 10 minutes at 4°C, and the supernatants were collected. The samples were analyzed with a rat IL-1β enzyme-linked immunosorbent assay kit (Multisciences Biotech, Hangzhou, China) at an absorbance of 450 nm on a spectrophotometer. IL-1β concentrations were determined from a standard curve.

Cell isolation, culture, and treatment

Rat spinal cord microvascular pericytes were isolated as previously described (Wu et al., 2015). Briefly, following decapitation (3–5 weeks of age, specific-pathogen-free grade, purchased from HuaXing Company, Zhengzhou, China, license No. SCXK (Yu) 2019-0002), the spinal column was isolated and immersed in pre-cooled PBS. After removing the meninges and large vessels, the gray matter of the spinal cord was separated and digested in DMEM containing collagenase type II (1 mg/mL; Worthington, Lakewood, NJ, USA) and DNase I (15 μg/mL; Sigma-Aldrich) for 1.5 hours at 37°C. The microvessel fragments were centrifuged in 20% bovine serum albumin/DMEM at 1000 × *g* for 20 minutes to adsorb the myelin. Collagenase/dispase (1 mg/mL; Roche, Basel, Switzerland) and DNase I (6.7 μg/mL) in DMEM were added and incubated for 1 hour at 37°C. The microvessel clusters were separated on a 33% continuous Percoll (GE Healthcare, Pittsburgh, PA, USA) gradient to remove endothelial cells. After washing twice in DMEM, the microvessels were collected in a culture dish containing complete medium, and the supernatant was replaced every 2 days. Pericytes in the microvascular fragment migrated out and proliferated. Pericytes with a purity > 90% were obtained by passage. The 3rd to 8th passages were used.

Pericytes were divided into sham, EXO, IFN-γ + TNF-α + LPS + Lipo + ATP, and IFN-γ + TNF-α + LPS + Lipo + ATP + EXO groups. Pericytes were pre-treated with interferon-γ (IFN-γ; 100 ng/mL; PeproTech China, Suzhou, China) + tumor necrosis factor α (TNF-α; 10 ng/mL; PeproTech) for 3 hours, then transfected with lipopolysaccharide (LPS; 1 μg/mL; Sigma-Aldrich) using Lipofectamine 3000 (Invitrogen) and co-incubated with or without adenosine triphosphate (ATP; 5 mM; Solarbio) for 4, 16 or 24 hours. Lipofectamine 3000 was used at a concentration of 5 μL/2 mL medium and premixed with LPS in DMEM for 15 minutes. When testing the protective effect of BMSCs-EXOs on pericytes, cells were co-incubated with or without BMSCs-EXOs (100 μg/mL) for 8 hours before exposure to a compound stimulus of IFN-γ + TNF-α + LPS + Lipo + ATP.

Methylthiazolyldiphenyl-tetrazolium bromide (MTT) assay

The viability of pericytes was evaluated with MTT (Amersco Grade, Shanghai, China) according to the manufacturers' protocols (Yu et al., 2019). Pericytes were seeded into 96-well plates at 5000 cells per well. After incubation, the supernatant was discarded and replaced with fresh culture medium. Thereafter, MTT, at a concentration of 5 mg/mL in PBS, was added to the medium, 20 μL per well, and incubated for 3 hours in the culture chamber. Next, dimethyl sulfoxide (Solarbio) was added at 150 μL per well for 10 minutes. Finally, optical absorbance was read at 562 nm using a SpectraMax Absorbance Reader (Molecular Devices, Silicon Valley, CA, USA).

Double staining with Hoechst 33342 and propidium iodide

Pericytes were co-incubated with propidium iodide (PI; 5 μg/mL; BioLegend, Shanghai, China) and Hoechst 33342 (1 μg/mL; Solarbio) for 15 minutes in a cell incubator, and then washed with PBS three times. Images were acquired using an inverted fluorescence microscope (BX53; Olympus).

Western blot assay

Total protein was extracted from pericytes using radio immunoprecipitation assay reagent (Beyotime Biotechnology, Shanghai, China) containing 100 μg/mL phenylmethylsulfonyl fluoride (Solarbio) and quantified using a bicinchoninic acid protein assay kit (Solarbio). Protein samples were denatured, separated by sodium dodecyl sulfate-polyacrylamide gel electrophoresis, and transferred onto a polyvinylidene fluoride membrane (EMD Millipore Corp., Burlington, MA, USA). The membranes were then blocked with a blocking solution (QuickBlock, Beyotime Biotechnology) at room temperature for 30 minutes, and then incubated with primary antibody against pro-caspase-1 (1:1000, rabbit, Cat# ab179515, Abcam), Nod1 (1:500, mouse, Cat#sc-398696, Santa Cruz), IL-1β (1:500, rabbit, Cat# ab9722, Abcam), CD9 (1:2000, rabbit, Cat# ab92726, Abcam), CD81 (1:5000, rabbit, Cat# ab109201, Abcam), CD63 (1:500, mouse, Cat#sc-5275, Santa Cruz) or glyceraldehyde-3-phosphate dehydrogenase (GAPDH; mouse, 1:1,0000, Cat# AC033, ABclonal, Wuhan, China) at 4°C overnight. The membranes were incubated with secondary goat anti-rabbit or mouse horseradish peroxidase-linked antibody (1:1000, Abbkine, Cat# A21220 or Cat# A25012) at room temperature for 1 hour. Finally, target bands were visualized using an enhanced chemiluminescence western blot kit (Thermo Fisher Scientific) and semi-quantified using ImageJ software.

Statistical analysis

Data are presented as mean ± standard deviation (SD). Group differences were determined by Student's *t*-test using SPSS 23.0 (IBM, Armonk, NY, USA). $P < 0.05$ was considered statistically significant.

Results

Characterization and tracing of BMSC-EXOs

To characterize the exosomes derived from BMSCs, they were isolated and purified from culture supernatants by ultracentrifugation, and then observed by transmission electron microscopy, which revealed numerous saucer-shaped vesicles (**Figure 1A** and **B**). Specimens prepared by the floating method were more stereoscopic and had a clearer morphology than those prepared by the dripping method. Nanoparticle tracking analysis revealed a particle size of approximately 100 nm in diameter (**Figure 1C**). In addition, western blot analysis confirmed distinctive exosome markers, including CD9, CD63 and CD81 (**Figure 1D**). For tracking, BMSC-EXOs were labeled with PKH26 dye. BMSC-EXOs were found at spinal cord lesion sites at 3 dpi and were assimilated by pericytes 6 hours after incubation *in vitro* (**Figure 1E** and **F**).

BMSC-EXOs reduce neuron death, decrease neural fiber degeneration, and improve locomotor functional recovery after SCI

To examine the effects of the injection of BMSC-EXOs on SCI-related pathology, a series of histological analyses at 3 dpi were conducted. We first performed Nissl staining to assess the survival of neurons on adjacent paraffin sections of the spinal cord. Structurally intact and deeply stained Nissl bodies were observed in the Sham and EXO groups. In the SCI group, a number of neurons exhibited karyopyknosis and even loss of Nissl bodies. The morphology and number of Nissl bodies in the SCI + EXO group was dramatically ameliorated compared with the SCI group (**Figure 2A**). Next, FJB staining was used to detect neuronal death in the spinal cord lesion core. Few FJB-positive cells were observed in the Sham and EXO groups. In the SCI group, the lesion region contained many FJB-positive cells. Notably, the numbers of FJB-positive cells were reduced after

BMSC-EXO treatment ($P < 0.05$, *vs*. SCI group; **Figure 2B** and **F**).

Luxol Fast Blue staining was carried out to evaluate the demyelination of neural fibers (Fan et al., 2020). The Sham and EXO groups exhibited blue staining of the regular structure of the myelin sheath. Severe perturbation of myelin arrangement along with myelin loss was observed in the SCI group. These defects were improved in the BMSC-EXOs group compared with the SCI group (**Figure 2C**).

NF-200 is an important neurofilament found specifically in neuronal cell bodies and axons, and its expression indirectly reflects the degree of axonal damage and repair after SCI (Trojanowski et al., 1986). Therefore, we used immunohistochemical staining to observe the changes in NF-200-positive axons. Significant differences were observed between the Sham and SCI groups. Furthermore, the expression of NF-200 was increased in the SCI + EXO group compared with the SCI group, suggesting that BMSC-EXOs inhibit axonal degeneration (**Figure 2D**). In addition, hematoxylin and eosin staining was used to assess overall damage. As shown in **Figure 2E**, the Sham and EXO groups exhibited normal motor neurons and Nissl bodies. Severe structural damage was observed in the SCI group, which was ameliorated by treatment with BMSC-EXOs.

Following SCI, the rats displayed obvious behavioral deficiencies. To further examine the effects of BMSC-EXOs on locomotor functional recovery after injury, BBB scores were recorded. BMSC-EXOs treatment improved locomotor function from 2 weeks post-SCI, compared with the SCI group (**Figure 2G**). These results demonstrate that BMSC-EXOs accelerate locomotor functional recovery in rats with SCI.

BMSC-EXOs attenuate BSCB leakage and reduce edema after SCI by inhibiting pyroptosis in pericytes

Studies have shown that traumatic SCI induces microvascular dysfunction and persistent BSCB disruption (Yu et al., 2016; Li et al., 2020). BSCB permeability was evaluated using the EB extravasation assay at 3 dpi. As shown in **Figure 3**, the infiltration of EB, fluorescence intensity of tissue and water content were low in the Sham and EXO groups. Compared with the high level of infiltration in the SCI group, EB infiltration was significantly reduced in the SCI + EXO group ($P < 0.05$; **Figure 3A**, **B** and **D**). Consistent with this, IVIS images showed evident increases in the fluorescence intensity of the surrounding tissue in the SCI group, which was lessened by BMSC-EXO administration (**Figure 3C**). In addition, the water content of spinal cord tissues was decreased in SCI rats administered BMSC-EXOs ($P < 0.05$; **Figure 3E**). These results suggest that BMSC-EXOs help maintain BSCB integrity.

To clarify the molecular mechanisms underlying the protective effects of BMSC-EXOs on BSCB integrity, we performed immunofluorescence staining for Pdgfr-β/caspase 1. Compared with the sham group, the co-localization of Pdgfr-β and caspase 1, as well as immunoreactivity for caspase 1, were increased in spinal cord tissue in SCI rats (**Figure 4A**). Notably, caspase 1 immunoreactivity was weak in pericytes in the SCI + EXOs group compared with the SCI group. The innate immune response is the first line of defense against microbial pathogens and endogenous stress, and pattern recognition receptors are the key to this nonspecific response. Nod1 is a pattern recognition receptor localized in the cytoplasm, and can activate caspase 1 and the cell death pathway (Clarke and Weiser, 2011). Western blot analysis showed that levels of Nod1 and pro-caspase 1 were significantly increased in spinal cord lesions compared with the sham group, and that BMSC-EXO treatment could reverse these changes ($P < 0.05$; **Figure 4B** and **C**). Moreover, IL-1β in the SCI + EXOs group was markedly lower than in the SCI group ($P < 0.05$, **Figure 4D**). Thus, we reasoned that pyroptosis-induced pericyte loss might be responsible for BSCB disruption.

To further elucidate the mechanisms of BSCB disruption, double immunofluorescence staining for Pdgfr-β and CD31 (pericyte/endothelial cell) was carried out. As shown in **Figure 4**, a marked loss of pericyte coverage on the vascular wall was observed in the spinal cord of SCI rats at 72 hours post-surgery. Notably, pericyte/endothelial cell coverage was evidently elevated in the SCI + EXO group compared with the SCI group ($P < 0.05$; **Figure 4E** and **F**). Taken together, these findings provide strong evidence that BMSC-EXO treatment results in decreased pericyte loss on the microvessels, thereby reducing BSCB leakage and edema after SCI.

A compound stimulus induces pyroptosis in pericytes *in vitro*

A recent study showed that pyroptosis in pericytes is activated by intracellular LPS (Nyúl-Tóth et al., 2017), distinct from the activation of other cell types such as astrocytes and BV2 cells (Adamczak et al., 2014; Nyúl-Tóth et al., 2017; Wilson et al., 2017). Double fluorescence staining with Hoechst and PI was performed to assess cell death. In the Sham and ATP groups, the cells were healthy, with only a few dead cells. We examined the effects of a combined stimulus of IFN-γ, TNF-α and LPS delivered using Lipofectamine 3000. This caused pro-caspase 1 activation in pericytes. However, after stimulation for 24 hours, cell viability was reduced only slightly and cell death was induced only weakly, which does not conform with the low rate of pericyte/endothelial cell coverage in SCI models. ATP is released by bacteria and the host during bacterial infection and sterile tissue damage, and may promote cell pyroptosis through excitation of the AMPK pathway and inflammasome activation (Zha et al., 2016). On the basis of previous studies, we primed pericytes with IFN-γ + TNF-α for 4 hours. When delivering LPS into pericytes using Lipofectamine 3000, ATP was added simultaneously for different intervals. We observed a marked decrease in cell viability and an increase in cell death at 16 and 24 hours, corresponding to a higher expression of pro-caspase 1 ($P < 0.05$; **Figure 5**). Thus, we chose this model to examine the protective effect of BMSC-EXOs on pericyte injury *in vitro*.

BMSC-EXOs provide cytoprotection against pyroptosis in pericytes *in vitro*

To further clarify whether BMSC-EXOs participate in cytoprotection against pyroptosis in pericytes *in vitro*, and to elucidate the underlying molecular mechanisms, pericytes were coincubated with BMSC-EXOs before exposure to the combined stimulus. The cells appeared healthy, with only a few dead cells in the Sham and EXO groups. BMSC-EXOs reversed the cell viability reduction, and decreased the number of PI-positive cells in rats with SCI ($P < 0.05$; **Figure 6A**, **B** and **D**). Nod1 and caspase 1 co-localization is an indication of inflammasome activation. BMSC-EXOs returned the inflammasome to a relatively low activation state (**Figure 6C**). Western blot analysis showed that the compound stimulus elevated the levels of Nod1, pro-caspase 1 and cleaved-IL-1β, reflecting the pyroptosis of pericytes. BMSC-EXO treatment reversed these changes ($P < 0.05$; **Figure 6E** and **F**).

Discussion

Accumulating evidence shows that exosomes derived from various stem cells exert neuroprotective effects in various disease models (Perets et al., 2018; Singla et al., 2019). Direct stem cell transplantation shows no significant differences in therapeutic effectiveness compared with transplantation of exosomes (Zhang et al., 2018; Xian et al., 2019). Exosomes have thus become a potential alternative to stem cell transplantation, and accordingly, BMSC-EXOs were investigated as a treatment for SCI in this study. Our findings clearly demonstrate that treatment with BMSC-EXOs reduces pericyte pyroptosis and improves survival following a compound stimulus challenge *in vitro*. Furthermore, BMSC-EXO administration not only maintained BSCB integrity by

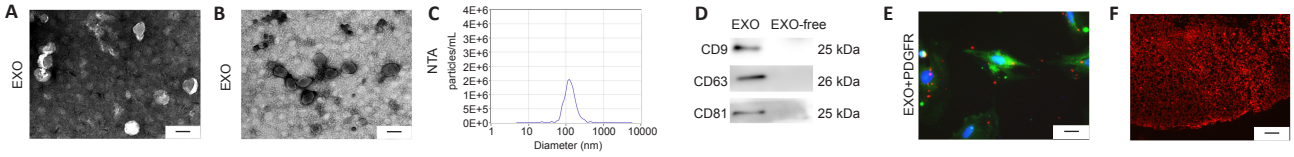

Figure 1 | **Characterization and tracing of BMSC-EXOs.**
(A–D) Morphology (A, floating method; B, dripping method), nanoparticle size distribution (C), and marker detection for BMSC-EXOs. Exosomes prepared by the floating method were more stereoscopic and clearer in morphology than those prepared by the dripping method. (D–F) Western blot, transmission electron microscope, and nanoparticle tracking analysis of BMSC-EXOs. (E) BMSC-EXOs labeled for PKH26 were observed using immunofluorescence in pericytes cultured for 6 hours *in vitro*. (F) BMSC-EXOs were found in spinal cord lesions 3 days after SCI. Scale bars: 20 μm in E, 100 nm in A, B; 200 μm in F. BMSC-EXOs: Bone mesenchymal stem cell-derived exosomes; EXO: exosome; PDGFR: platelet-derived growth factor receptor.

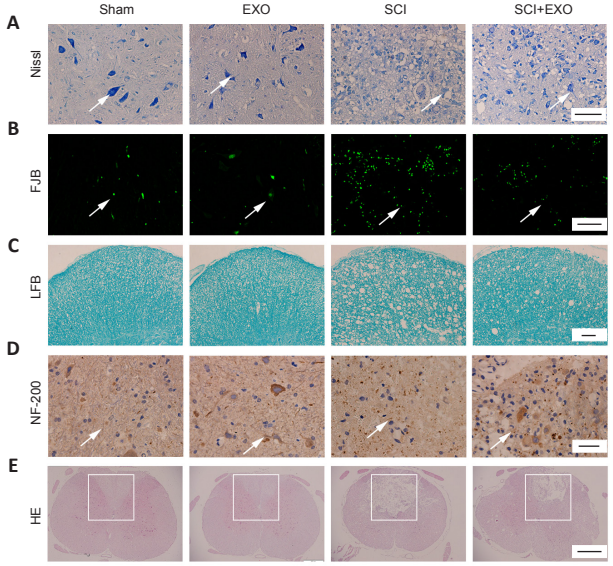

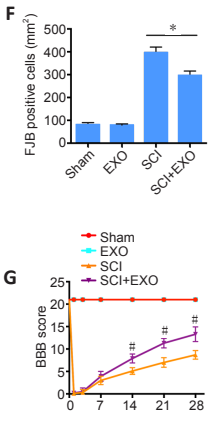

Figure 2 | **BMSC-EXOs reduce the lesion and improve locomotor functional recovery after SCI.**
(A) Nissl staining of spinal cord 72 hours post-SCI. Arrows indicate Nissl-positive cells. (B) FJB staining around the injured lesion at 3 dpi. Arrows indicate FJB-positive cells. (C) LFB staining in spinal cord at 72 hours. (D) Immunohistochemistry for NF-200 (arrows) in spinal cord tissue after severe injury. (E) HE staining in spinal cord 3 dpi. The rectangle indicates the location of the damage. Compared with the sham group, the SCI group showed loss of Nissl bodies, more FJB-positive cells, disordered myelin arrangement, lightly-stained nerve fibers, and severe structural damage. Exosome treatment reversed these pathological changes. Scale bars: 50 μm in A, B, D; 100 μm in C; 500 μm in E. (F) Quantitative analysis of FJB-positive cells. (G) BBB scores post-SCI. Data are expressed as the mean ± SD (n = 6 in F and 10 in G). *P < 0.05; #P < 0.05 *vs.* SCI group (Student's t-test). BBB: Basso, Beattie and Bresnahan; BMSC-EXO: bone mesenchymal stem cell-derived exosome; dpi: days post injury; EXO: exosome; FJB: Fluoro-Jade B; HE: hematoxylin and eosin; LFB: Luxol Fast Blue; NF-200: neurofilament 200; SCI: spinal cord injury.

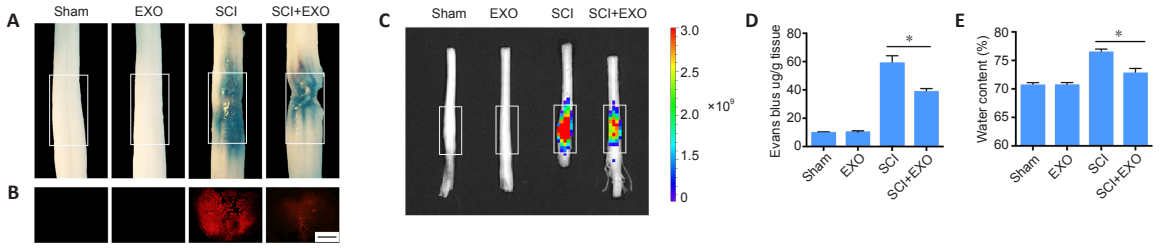

Figure 3 | **BMSC-EXOs preserve blood-spinal cord barrier integrity and reduce edema post-SCI.**
(A) Macroscopic images of Evans blue extravasation photographed at 3 dpi. The rectangle indicates the location of the damage. (B) Fluorescence microscopy images of Evans blue leakage at 3 dpi. Scale bar: 1 mm. (C) IVIS images of spinal cord stripped from the spine at 3 dpi. Compared with the Sham and EXO groups, the SCI group showed severe injury with higher EB content in A, and stronger fluorescence intensity in B and C. Exosome treatment reversed these changes. The rectangle indicates the location of the damage. (D) Quantitative analysis of Evans blue leakage. (E) Quantification of spinal cord water content at 3 dpi. Data are expressed as the mean ± SD (n = 6). *P < 0.05 (Student's t-test). BMSC-EXO: Bone mesenchymal stem cell-derived exosome; dpi: days post injury; EXO: exosome; IVIS: *In Vivo* Imaging System; SCI: spinal cord injury.

inhibiting pericyte pyroptosis, but also promoted neuronal survival, fiber regeneration, and functional recovery in the SCI model.

The BSCB is of critical importance in maintaining the fluid microenvironment of the spinal cord within narrow limits (Albayar et al., 2019). Pericytes wrap around the capillaries and share a common basement membrane with microvascular endothelial cells (Bang et al., 2017). The interaction between pericytes and neighboring cells is essential for angiogenesis, angioarchitecture, vascular stability, and BBB/BSCB formation and maintenance (Bernacki et al., 2008; Bhowmick et al., 2019; Courtney and Sutherland, 2020). A large number of studies have advanced our understanding of the detrimental effect of pericyte loss on BSCB permeability in diverse diseases, including multiple sclerosis, amyotrophic lateral sclerosis and SCI (Wu et al., 2014; Garbuzova-Davis et al., 2019; Uchida et al., 2019). Previous studies have shown that traumatic insults to the spinal cord invariably lead to pericyte injury, disruption of microvascular stability, and a dramatic increase in BSCB leakage (Figley et al., 2014). Therefore, to improve motor functional recovery, it is imperative to protect pericytes from pathological insults and preserve BSCB integrity. Consistent with the results of others, we found increased permeability of the BSCB and severe tissue edema after SCI. Furthermore, our findings demonstrate that BMSC-EXOs can reverse BSCB leakage and reduce edema by inhibiting pericyte pyroptosis, thereby improving pericyte/endothelial cell coverage and resulting in better functional recovery after injury.

Pyroptosis is a unique type of cell death, characterized by the activation of caspase 1, the formation of discrete pores in the cytomembrane, and the maturation and release of inflammatory cytokines such as IL-1β. When cells are subjected to pathological insult, such as ischemia-reperfusion and microbial infection, pyroptosis is induced. Several major cell types in the central nervous system have been reported to undergo pyroptosis, including microglia, endothelial cells and astrocytes (Abulafia et al., 2009; Minkiewicz et al., 2013; Adamczak et al., 2014). Furthermore, previous

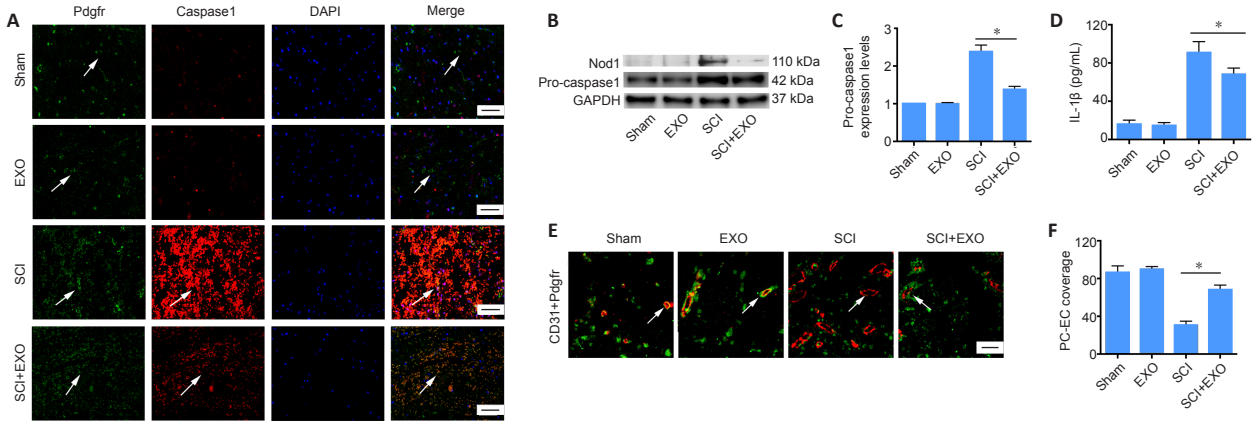

Figure 4 | **BMSC-EXOs decrease pyroptosis in pericytes and increase pericyte coverage *in vivo*.**
(A) Colocalization of Pdgfr and caspase 1 in the spinal cord at 3 dpi. Arrows indicate pericytes. Red: DyLight 594, caspase 1; green: DyLight 488, Pdgfr; blue: DAPI. (B, C) Expression of Nod1 (data not shown) and pro-caspase 1 (fold-change compared with the Sham group) assessed by western blot assay. (D) Expression of IL-1β assessed by enzyme-linked immunosorbent assay. (E) Representative immunofluorescence images of Pdgfrβ$^+$ pericytes and CD31$^+$ endothelial cells after SCI. Compared with the Sham and EXO groups, the SCI group showed loss of pericytes and low PC/EC coverage. Exosome treatment reduced these changes. Arrows indicate microvessels. Red: DyLight 594, CD31$^+$ endothelial cells; green: DyLight 488, Pdgfrβ+ pericytes; blue: DAPI. Nuclei were labeled with DAPI. Scale bars: 50 μm in A, and 20 μm in E. (F) Percentage of PC/EC coverage in spinal cord microvessels. Data are expressed as the mean ± SD (n = 3 in C, n = 6 in D and F). *P < 0.05 (Student's t-test). BMSC-EXO: Bone mesenchymal stem cell-derived exosome; DAPI: 4′,6-diamidino-2-phenylindole; EXO: exosome; PC/EC: pericyte/endothelial cell; Pdgfr: platelet-derived growth factor receptor; SCI: spinal cord injury.

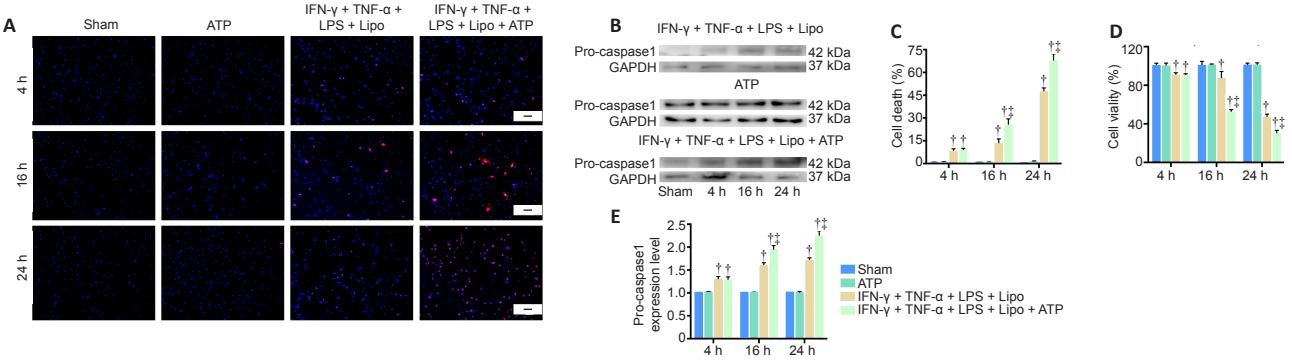

Figure 5 | **Compound stimulus induces pyroptosis in pericytes *in vitro*.**
(A) Double staining for propidium iodide and Hoechst 33342 in pericytes. Scale bars: 100 μm. (B, E) Expression of pro-caspase 1 (fold change to sham group) was assessed by western blot. (C) The dead cells in cultured pericytes were detected using Hoechst 33342/PI. (D) Cell viability was assessed by the MTT assay. Data are presented as mean ± SD. The experiment was repeated six, six and three times in C, D and E, respectively. †P < 0.05, *vs*. ATP group; ‡P < 0.05, *vs*. IFN-γ + TNF-α + LPS + Lipo group (Student's t-test). IFN-γ: Interferon-γ; Lipo: Lipofectamine 3000; LPS: lipopolysaccharide; MTT: methylthiazolyldiphenyl-tetrazolium bromide; TNF-α: tumor necrosis factor α.

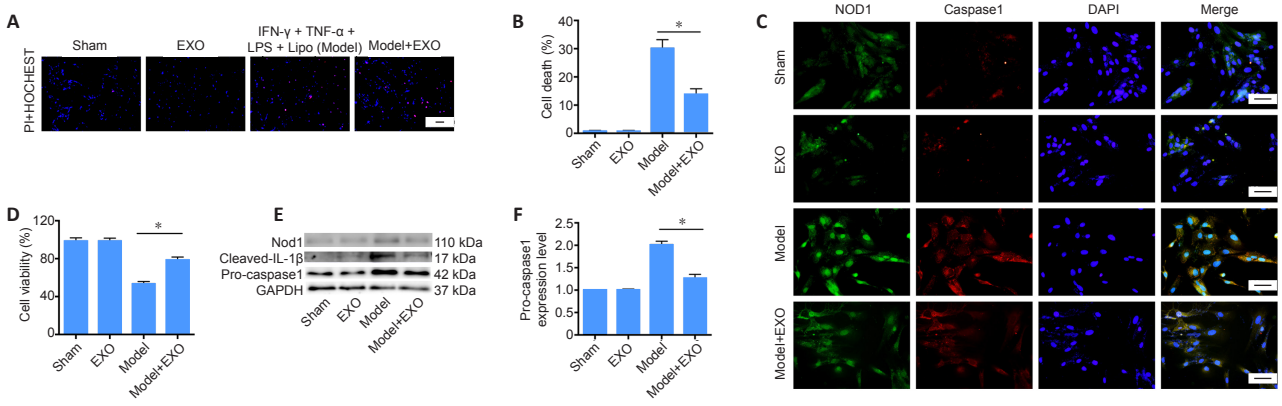

Figure 6 | **BMSC-EXOs provide cytoprotection against pyroptosis in pericytes in vitro by inhibiting Nod1 inflammasome activation.**
(A, B) Representative fluorescence images of Hoechst 33342 and PI in pericytes, indicating cell death. Cells in the Sham and EXO group are in good condition, with few dead cells. In contrast, the model group showed increased cell death and decreased cell viability. Exosome treatment ameliorated these changes. (C) Cultured pericytes labeled with Nod1 and caspase 1. Compared with the Sham and EXO groups, the SCI group showed higher expression of Nod1 and caspase 1. Exosome treatment reduced their expression. Red: DyLight 594, caspase 1; green: DyLight 488, Nod1; blue: DAPI. Nuclei were stained with DAPI. Scale bars: 100 μm in A, 50 μm in C. (D) MTT analysis of cell viability. (E, F) The expression levels of Nod1, pro-caspase 1 and cleaved IL-1β were determined by western blot assay. Data are shown as mean ± SD. The experiment was repeated six times in B–D, and six times in E and F. *P < 0.05 (Student's t-test). BMSC-EXOs: Exosomes derived from bone mesenchymal stem cells; DAPI: 4′,6-diamidino-2-phenylindole; EXO: exosome; IFN-γ: interferon-γ; Lipo: Lipofectamine 3000; LPS: lipopolysaccharide; MTT: methylthiazolyldiphenyl-tetrazolium bromide; PI: propidium iodide; TNF-α: tumor necrosis factor α.

studies have shown that caspase 1 downregulation inhibits inflammasome assembly and pyroptosis in several disease models, including SCI, epilepsy, Alzheimer's disease and multiple sclerosis, which are associated with neuronal injury and neuroinflammation (Tan et al., 2015; McKenzie et al., 2018). Hence, targeting the regulation of cellular pyroptosis may allow us to regulate disease pathological processes. Our results suggest that compared with the IFN-γ + TNF-α + LPS + Lipo group, a combined stimulus of IFN-γ + TNF-α + LPS + Lipo + ATP significantly enhances the expression of caspase 1 and robustly induces pericyte death, which may better simulate the internal environment of the body under pathological conditions. Furthermore, pericyte death caused by caspase 1-mediated activation of the classical pyroptosis pathway aggravated BSCB breakdown in the SCI model. Strikingly, these pathological changes and motor dysfunction after SCI were ameliorated by administration of exosomes.

Emerging evidence shows a protective effect of Nod1 in the central nervous system. A previous study demonstrated that Nod1 protects mice from infection by L. monocytogenes and inhibits intracellular bacterial growth in different cell types, including astrocytes and fibroblasts (Mosa et al., 2009). A recent study showed that activation of infiltrating dendritic cells may participate in the pathologic changes in experimental autoimmune encephalomyelitis via RIP2-, NOD1- and NOD2-mediated pathways (Shaw et al., 2011). Additionally, previous studies reported that there is no canonical activation of NLRP1, NLRP2, NLRP3 or NLRC4 inflammasomes, but only non-canonical activation of Nod1, Nod2 and TLR2 in human brain pericytes (Nyúl-Tóth et al., 2017). Thus, we chose to detect Nod1 expression in pericytes after treatment with the various drugs.

In our study, Nod1 in pericytes was markedly upregulated after exposure to IFN-γ + TNF-α + LPS + Lipo + ATP. Furthermore, the upregulation of pro-caspase 1 and the release of IL-1β inhibited the survival of pericytes. Our findings indicate for the first time that exosome treatment effectively inhibits pyroptosis in pericytes by inhibiting the Nod1 inflammasome. These findings suggest that BSCB integrity is improved by exosomes post-SCI by the inhibition of pericyte pyroptosis.

There are limitations to this study. Exosomes derived from BMSCs contain DNA, mRNA, miRNA, lncRNA, proteins and lipomolecules, which can be transferred and subsequently influence signaling pathways in recipient cells (Raposo and Stoorvogel, 2013). A recent study showed that exosomes, extracted from the supernatant of miR-21-modified MSCs, improved the survival of neurons and promoted functional recovery after SCI via the miR-21/PTEN/PDCD4 signaling pathway (Kang et al., 2019). Further study is needed to identify the exosomal components involved in regulating pericyte pyroptosis. However, it would have been highly informative for using exosomes derived from a non-BMSC source, for comparison. It is possible that the protective effects of the BMSC-derived exosomes could be mimicked by exosomes from another cell type, such as placental mesenchymal stem cells.

Our novel findings collectively suggest that BMSC-EXOs significantly promote the survival of pericytes by modulating NOD1-related signaling pathways *in vitro*. BMSC-EXOs effectively suppress pericytes pyroptosis and maintain BSCB integrity, thereby enhancing recovery following SCI. Thus, BMSC-EXOs may have therapeutic potential in neuroprotection in SCI.

Author contributions: *Study design: LLW, YZ, YJJ; SCI model establishment and BBB score assessment: KMW, RRD; molecular biology: YBY, LJJ; data collection and statistical analysis: LLW, ZG; manuscript writing: ZG, JFT. All authors reviewed and approved the manuscript.*

Conflicts of interest: *The authors declare that they have no conflicts of interest.*

Financial support: *This work was supported by the National Natural Science Foundation of China, No. U1604170 (to YJJ). The funding source had no role in study conception and design, data analysis or interpretation, paper writing or deciding to submit this paper for publication.*

Institutional review board statement: *This study was approved by the Animal Ethics Committee of Zhengzhou University on March 16, 2019.*

Data sharing statement: *Datasets analyzed during the current study are available from the corresponding author on reasonable request.*

Plagiarism check: *Checked twice by iThenticate.*

Peer review: *Externally peer reviewed.*

References

Abulafia DP, de Rivero Vaccari JP, Lozano JD, Lotocki G, Keane RW, Dietrich WD (2009) Inhibition of the inflammasome complex reduces the inflammatory response after thromboembolic stroke in mice. J Cereb Blood Flow Metab 29:534-544.

Adamczak SE, de Rivero Vaccari JP, Dale G, Brand FJ, 3rd, Nonner D, Bullock MR, Dahl GP, Dietrich WD, Keane RW (2014) Pyroptotic neuronal cell death mediated by the AIM2 inflammasome. J Cereb Blood Flow Metab 34:621-629.

Albayar AA, Roche A, Swiatkowski P, Antar S, Ouda N, Emara E, Smith DH, Ozturk AK, Awad BI (2019) Biomarkers in spinal cord injury: prognostic insights and future potentials. Front Neurol 10:27.

Amtul Z, Najdat AN, Hill DJ, Arany EJ (2021) Differential temporal and spatial post-injury alterations in cerebral cell morphology and viability. J Comp Neurol 529:421-433.

Aslan A, Cemek M, Buyukokuroglu ME, Altunbas K, Bas O, Yurumez Y, Cosar M (2009) Dantrolene can reduce secondary damage after spinal cord injury. Eur Spine J 18:1442-1451.

Bang S, Lee SR, Ko J, Son K, Tahk D, Ahn J, Im C, Jeon NL (2017) A low permeability microfluidic blood-brain barrier platform with direct contact between perfusable vascular network and astrocytes. Sci Rep 7:8083.

Basso DM, Beattie MS, Bresnahan JC (1995) A sensitive and reliable locomotor rating scale for open field testing in rats. J Neurotrauma 12:1-21.

Bergsbaken T, Fink SL, Cookson BT (2009) Pyroptosis: host cell death and inflammation. Nat Rev Microbiol 7:99-109.

Bernacki J, Dobrowolska A, Nierwińska K, Małecki A (2008) Physiology and pharmacological role of the blood-brain barrier. Pharmacol Rep 60:600-622.

Berthiaume AA, Hartmann DA, Majesky MW, Bhat NR, Shih AY (2018) Pericyte structural remodeling in cerebrovascular health and homeostasis. Front Aging Neurosci 10:210.

Bhowmick S, D'Mello V, Caruso D, Wallerstein A, Abdul-Muneer PM (2019) Impairment of pericyte-endothelium crosstalk leads to blood-brain barrier dysfunction following traumatic brain injury. Exp Neurol 317:260-270.

Clarke TB, Weiser JN (2011) Intracellular sensors of extracellular bacteria. Immunol Rev 243:9-25.

Courtney JM, Sutherland BA (2020) Harnessing the stem cell properties of pericytes to repair the brain. Neural Regen Res 15:1021-1022.

Dai W, Wang X, Teng H, Li C, Wang B, Wang J (2019) Celastrol inhibits microglial pyroptosis and attenuates inflammatory reaction in acute spinal cord injury rats. Int Immunopharmacol 66:215-223.

David S, Kroner A (2011) Repertoire of microglial and macrophage responses after spinal cord injury. Nat Rev Neurosci 12:388-399.

Fan H, Tang HB, Chen Z, Wang HQ, Zhang L, Jiang Y, Li T, Yang CF, Wang XY, Li X, Wu SX, Zhang GL (2020) Inhibiting HMGB1-RAGE axis prevents pro-inflammatory macrophages/microglia polarization and affords neuroprotection after spinal cord injury. J Neuroinflammation 17:295.

Figley SA, Khosravi R, Legasto JM, Tseng YF, Fehlings MG (2014) Characterization of vascular disruption and blood-spinal cord barrier permeability following traumatic spinal cord injury. J Neurotrauma 31:541-552.

Gao W, Li F, Liu L, Xu X, Zhang B, Wu Y, Yin D, Zhou S, Sun D, Huang Y, Zhang J (2018) Endothelial colony-forming cell-derived exosomes restore blood-brain barrier continuity in mice subjected to traumatic brain injury. Exp Neurol 307:99-108.

Garbuzova-Davis S, Ehrhart J, Mustafa H, Llauget A, Boccio KJ, Sanberg PR, Appel SH, Borlongan CV (2019) Phenotypic characteristics of human bone marrow-derived endothelial progenitor cells in vitro support cell effectiveness for repair of the blood-spinal cord barrier in ALS. Brain Res 1724:146428.

Haque A, Capone M, Matzelle D, Cox A, Banik NL (2017) Targeting enolase in reducing secondary damage in acute spinal cord injury in rats. Neurochem Res 42:2777-2787.

Hashitani H, Mitsui R (2019) Role of pericytes in the initiation and propagation of spontaneous activity in the microvasculature. Adv Exp Med Biol 1124:329-356.
Hashitani H, Mitsui R, Miwa-Nishimura K, Lam M (2018) Role of capillary pericytes in the integration of spontaneous Ca(2+) transients in the suburothelial microvasculature in situ of the mouse bladder. J Physiol 596:3531-3552.
Hoogduijn MJ, Roemeling-van Rhijn M, Korevaar SS, Engela AU, Weimar W, Baan CC (2011) Immunological aspects of allogeneic and autologous mesenchymal stem cell therapies. Hum Gene Ther 22:1587-1591.
Huang X, Ding J, Li Y, Liu W, Ji J, Wang H, Wang X (2018) Exosomes derived from PEDF modified adipose-derived mesenchymal stem cells ameliorate cerebral ischemia-reperfusion injury by regulation of autophagy and apoptosis. Exp Cell Res 371:269-277.
Kalani A, Tyagi N (2015) Exosomes in neurological disease, neuroprotection, repair and therapeutics: problems and perspectives. Neural Regen Res 10:1565-1567.
Kang J, Li Z, Zhi Z, Wang S, Xu G (2019) MiR-21 derived from the exosomes of MSCs regulates the death and differentiation of neurons in patients with spinal cord injury. Gene Ther 26:491-503.
Li C, Chen X, Qiao S, Liu X, Liu C, Zhu D, Su J, Wang Z (2014) Melatonin lowers edema after spinal cord injury. Neural Regen Res 9:2205-2210.
Li C, Jiao G, Wu W, Wang H, Ren S, Zhang L, Zhou H, Liu H, Chen Y (2019) Exosomes from bone marrow mesenchymal stem cells inhibit neuronal apoptosis and promote motor function recovery via the Wnt/β-catenin signaling pathway. Cell Transplant 28:1373-1383.
Li P, Zhou Y, Goodwin AJ, Cook JA, Halushka PV, Zhang XK, Wilson CL, Schnapp LM, Zingarelli B, Fan H (2018) Fli-1 governs pericyte dysfunction in a murine model of sepsis. J Infect Dis 218:1995-2005.
Li X, Luo D, Hou Y, Hou Y, Chen S, Zhan J, Luan J, Wang L, Lin D (2020) Sodium tanshinone IIA silate exerts microcirculation protective effects against spinal cord injury in vitro and in vivo. Oxid Med Cell Longev 2020:3949575.
Luo Y, Fu C, Wang Z, Zhang Z, Wang H, Liu Y (2015) Mangiferin attenuates contusive spinal cord injury in rats through the regulation of oxidative stress, inflammation and the Bcl-2 and Bax pathway. Mol Med Rep 12:7132-7138.
Mahmoudi M, Taghavi-Farahabadi M, Namaki S, Baghaei K, Rayzan E, Rezaei N, Hashemi SM (2019) Exosomes derived from mesenchymal stem cells improved function and survival of neutrophils from severe congenital neutropenia patients in vitro. Hum Immunol 80:990-998.
McKenzie BA, Mamik MK, Saito LB, Boghozian R, Monaco MC, Major EO, Lu JQ, Branton WG, Power C (2018) Caspase-1 inhibition prevents glial inflammasome activation and pyroptosis in models of multiple sclerosis. Proc Natl Acad Sci U S A 115:E6065-6074.
Minkiewicz J, de Rivero Vaccari JP, Keane RW (2013) Human astrocytes express a novel NLRP2 inflammasome. Glia 61:1113-1121.
Mosa A, Trumstedt C, Eriksson E, Soehnlein O, Heuts F, Janik K, Klos A, Dittrich-Breiholz O, Kracht M, Hidmark A, Wigzell H, Rottenberg ME (2009) Nonhematopoietic cells control the outcome of infection with Listeria monocytogenes in a nucleotide oligomerization domain 1-dependent manner. Infect Immun 77:2908-2918.
Moya A, Paquet J, Deschepper M, Larochette N, Oudina K, Denoeud C, Bensidhoum M, Logeart-Avramoglou D, Petite H (2018) Human mesenchymal stem cell failure to adapt to glucose shortage and rapidly use intracellular energy reserves through glycolysis explains poor cell survival after implantation. Stem Cells 36:363-376.
Nyúl-Tóth Á, Kozma M, Nagyőszi P, Nagy K, Fazakas C, Haskó J, Molnár K, Farkas AE, Végh AG, Váró G, Galajda P, Wilhelm I, Krizbai IA (2017) Expression of pattern recognition receptors and activation of the non-canonical inflammasome pathway in brain pericytes. Brain Behav Immun 64:220-231.
Orr MB, Gensel JC (2018) Spinal cord injury scarring and inflammation: therapies targeting glial and inflammatory responses. Neurotherapeutics 15:541-553.
Pan YL, Guo Y, Ma Y, Wang L, Zheng SY, Liu MM, Huang GC (2019) Aquaporin-4 expression dynamically varies after acute spinal cord injury-induced disruption of blood spinal cord barrier in rats. Neuropathology 39:181-186.
Perets N, Hertz S, London M, Offen D (2018) Intranasal administration of exosomes derived from mesenchymal stem cells ameliorates autistic-like behaviors of BTBR mice. Mol Autism 9:57.
Phinney DG, Di Giuseppe M, Njah J, Sala E, Shiva S, St Croix CM, Stolz DB, Watkins SC, Di YP, Leikauf GD, Kolls J, Riches DW, Deiuliis G, Kaminski N, Boregowda SV, McKenna DH, Ortiz LA (2015) Mesenchymal stem cells use extracellular vesicles to outsource mitophagy and shuttle microRNAs. Nat Commun 6:8472.
Rahimi-Movaghar V, Sayyah MK, Akbari H, Khorramirouz R, Rasouli MR, Moradi-Lakeh M, Shokraneh F, Vaccaro AR (2013) Epidemiology of traumatic spinal cord injury in developing countries: a systematic review. Neuroepidemiology 41:65-85.
Raposo G, Stoorvogel W (2013) Extracellular vesicles: exosomes, microvesicles, and friends. J Cell Biol 200:373-383.
Shaw PJ, Barr MJ, Lukens JR, McGargill MA, Chi H, Mak TW, Kanneganti TD (2011) Signaling via the RIP2 adaptor protein in central nervous system-infiltrating dendritic cells promotes inflammation and autoimmunity. Immunity 34:75-84.
Singla DK, Johnson TA, Tavakoli Dargani Z (2019) Exosome treatment enhances anti-inflammatory M2 macrophages and reduces inflammation-induced pyroptosis in doxorubicin-induced cardiomyopathy. Cells 8:1224.
Tan CC, Zhang JG, Tan MS, Chen H, Meng DW, Jiang T, Meng XF, Li Y, Sun Z, Li MM, Yu JT, Tan L (2015) NLRP1 inflammasome is activated in patients with medial temporal lobe epilepsy and contributes to neuronal pyroptosis in amygdala kindling-induced rat model. J Neuroinflammation 12:18.
Tan LL, Jiang XL, Xu LX, Li G, Feng CX, Ding X, Sun B, Qin ZH, Zhang ZB, Feng X, Li M (2021) TP53-induced glycolysis and apoptosis regulator alleviates hypoxia/ischemia-induced microglial pyroptosis and ischemic brain damage. Neural Regen Res 16:1037-1043.
Tavakoli Dargani Z, Singla DK (2019) Embryonic stem cell-derived exosomes inhibit doxorubicin-induced TLR4-NLRP3-mediated cell death-pyroptosis. Am J Physiol Heart Circ Physiol 317:H460-471.
Trojanowski JQ, Walkenstein N, Lee VM (1986) Expression of neurofilament subunits in neurons of the central and peripheral nervous system: an immunohistochemical study with monoclonal antibodies. J Neurosci 6:650-660.
Uchida Y, Sumiya T, Tachikawa M, Yamakawa T, Murata S, Yagi Y, Sato K, Stephan A, Ito K, Ohtsuki S, Couraud PO, Suzuki T, Terasaki T (2019) Involvement of claudin-11 in disruption of blood-brain,-spinal cord, and-arachnoid barriers in multiple sclerosis. Mol Neurobiol 56:2039-2056.
Ungerer G, Cui J, Ndam T, Bekemeier M, Song H, Li R, Siedhoff HR, Yang B, Appenteng MK, Greenlief CM, Miller DK, Sun GY, Folk WR, Gu Z (2020) Harpagophytum procumbens extract ameliorates allodynia and modulates oxidative and antioxidant stress pathways in a rat model of spinal cord injury. Neuromolecular Med 22:278-292.
Wang L, Pei S, Han L, Guo B, Li Y, Duan R, Yao Y, Xue B, Chen X, Jia Y (2018) Mesenchymal stem cell-derived exosomes reduce A1 astrocytes via downregulation of phosphorylated NFκB P65 subunit in spinal cord injury. Cell Physiol Biochem 50:1535-1559.
Wei H, Chen J, Wang S, Fu F, Zhu X, Wu C, Liu Z, Zhong G, Lin J (2019) A nanodrug consisting of doxorubicin and exosome derived from mesenchymal stem cells for osteosarcoma treatment in vitro. Int J Nanomedicine 14:8603-8610.
Wei YS, Liu HJ, Wang HF, Wang JD, Zhao WJ, Chen WP (2021) Cardiomyocyte-like differentiation of bone marrow mesenchymal stem cells induced by myocardial tissue lysates from different parts of the myocardium. Zhongguo Zuzhi 7Gongcheng Yanjiu 25:32-37.
Wilson JL, Bouillaud F, Almeida AS, Vieira HL, Ouidja MO, Dubois-Randé JL, Foresti R, Motterlini R (2017) Carbon monoxide reverses the metabolic adaptation of microglia cells to an inflammatory stimulus. Free Radic Biol Med 104:311-323.
Wu Q, Jing Y, Yuan X, Li B, Wang B, Liu M, Li H, Xiu R (2015) The distinct abilities of tube-formation and migration between brain and spinal cord microvascular pericytes in rats. Clin Hemorheol Microcirc 60:231-240.
Wu Q, Jing Y, Yuan X, Zhang X, Li B, Liu M, Wang B, Li H, Liu S, Xiu R (2014) Melatonin treatment protects against acute spinal cord injury-induced disruption of blood spinal cord barrier in mice. J Mol Neurosci 54:714-722.
Xian P, Hei Y, Wang R, Wang T, Yang J, Li J, Di Z, Liu Z, Baskys A, Liu W, Wu S, Long Q (2019) Mesenchymal stem cell-derived exosomes as a nanotherapeutic agent for amelioration of inflammation-induced astrocyte alterations in mice. Theranostics 9:5956-5975.
Xie M, Deng L, Yu Y, Xie X, Zhang M (2021) The effects of Bushen Yiqi Huoxue prescription and its disassembled prescriptions on a diabetic retinopathy model in Sprague Dawley rats. Biomed Pharmacother 133:110920.
Xiong Y, Mahmood A, Chopp M (2017) Emerging potential of exosomes for treatment of traumatic brain injury. Neural Regen Res 12:19-22.
Xu Y, He Q, Wang M, Wang X, Gong F, Bai L, Zhang J, Wang W (2019) Quantifying blood-brain-barrier leakage using a combination of evans blue and high molecular weight FITC-Dextran. J Neurosci Methods 325:108349.
Yaghoubi Y, Movassaghpour A, Zamani M, Talebi M, Mehdizadeh A, Yousefi M (2019) Human umbilical cord mesenchymal stem cells derived-exosomes in diseases treatment. Life Sci 233:116733.
Yi X, Wei X, Lv H, An Y, Li L, Lu P, Yang Y, Zhang Q, Yi H, Chen G (2019) Exosomes derived from microRNA-30b-3p-overexpressing mesenchymal stem cells protect against lipopolysaccharide-induced acute lung injury by inhibiting SAA3. Exp Cell Res 383:111454.
Yu Q, Huang J, Hu J, Zhu H (2016) Advance in spinal cord ischemia reperfusion injury: blood-spinal cord barrier and remote ischemic preconditioning. Life Sci 154:34-38.
Yu X, Zhang S, Zhao D, Zhang X, Xia C, Wang T, Zhang M, Liu T, Huang W, Wu B (2019) SIRT1 inhibits apoptosis in in vivo and in vitro models of spinal cord injury via microRNA-494. Int J Mol Med 43:1758-1768.
Zha QB, Wei HX, Li CG, Liang YD, Xu LH, Bai WJ, Pan H, He XH, Ouyang DY (2016) ATP-induced inflammasome activation and pyroptosis is regulated by AMP-activated protein kinase in macrophages. Front Immunol 7:597.
Zhang T, Li K, Zhang ZL, Gao K, Lv CL (2021) LncRNA Airsci increases the inflammatory response after spinal cord injury in rats through the nuclear factor kappa B signaling pathway. Neural Regen Res 16:772-777.
Zhang X, Liu J, Yu B, Ma F, Ren X, Li X (2018) Effects of mesenchymal stem cells and their exosomes on the healing of large and refractory macular holes. Graefes Arch Clin Exp Ophthalmol 256:2041-2052.
Zheng G, Zhan Y, Wang H, Luo Z, Zheng F, Zhou Y, Wu Y, Wang S, Wu Y, Xiang G, Xu C, Xu H, Tian N, Zhang X (2019) Carbon monoxide releasing molecule-3 alleviates neuron death after spinal cord injury via inflammasome regulation. EBioMedicine 40:643-654.

C-Editor: Zhao M; S-Editors: Yu J, Li CH; L-Editors: Patel B, Yu J, Song LP; T-Editor: Jia Y